

Real-time Control of Ship's Roll Motion with Gyrostabilizers

Lifen Hu¹, Ming Zhang², Xingxing Yu¹, Zhiming Yuan², Wubin Li³

1. Ulsan Ship and Ocean College, Ludong University, Yantai 264025, China; 2. Department of Naval Architecture, Ocean and Marine Engineering, University of Strathclyde, Glasgow G4 0LZ, UK; 3. Transportation School, Ludong University, Yantai 264025, China

Abstract:

The safety of ship manoeuvring operations is greatly affected by large roll motions under severe wave conditions. While existing studies have focused on optimizing hydrodynamic performance devices, these approaches may not be effective under realistic sea conditions where wave frequency and direction are irregular. Thus, predicting ship motion tendencies and implementing a reasonable control approach is crucial for improving ship safety. This study proposes a novel and practical control strategy that can effectively suppress roll motion of ships under realistic random wave conditions. The approach utilizes a real-time controller based on model predictive control (MPC) that is actuated by a dual gyrostabilizer. The ship's roll motion response in beam waves is calculated using one degree-of-freedom hydrodynamic modeling, and the wave memory effect is taken into consideration by employing system identification. A synthetic mathematical model of MPC and the dual gyrostabilizer method is introduced in state-space representation to compensate for wave excitation moment in real-time. The proposed method's efficacy is validated by comparing with a roll stabilization scenario of a particular ship in the literature, and control performance of a standard ship under regular and irregular wave conditions is separately discussed. Results indicate that the proposed method can significantly reduce roll motion amplitude and is feasible for nonlinear ship motion control problems. This study sheds light on the multi-degree-of-freedom motion control of ships under beam wave conditions.

Keywords: gyrostabiliser; irregular wave; model predictive control; roll motion control; state-space model

1 Introduction

When ships manoeuvre in waves, the motion amplitude may be larger in harsh conditions. In particular, a large roll motion poses potential risks to the ship's manoeuvre operations. Most of the existing studies have mostly focused on the optimizing hydrodynamic performance of equipment, i.e., bilge keels [Irkal, 2019], with the designers attempting to enhance ship safety during the design stage [Kang, 2013]. However, under realistic sea conditions where wave frequency and direction are both irregular, it may not be practically feasible to reduce roll motion. If a reasonable strategy or system could be adopted to control the ship motion in waves, ship safety would be greatly improved. To effectively control roll motion, we must obtain the ship's motion response parameters.

At present, there are two commonly used methods for calculating ship motion response: one is the computational fluid dynamics (CFD) method, which aims to solve the Navier–Stokes (NS) equation that comprehensively describes the flow field in detail, and consider the fluid viscosity and nonlinearity of interaction between ships and waves [Gao, 2020; Hu, 2021]. However, this method has strict calculation requirements to obtain more accurate results [Ruth, 2019], leading to excessive computational time and potentially limited range of applications. On the other hand, due to its high calculation efficiency, potential flow theory is widely used to

solve the ship motion response model, originally developed to solve seakeeping problems and obtain the dynamic characteristics of floating bodies in waves [Li, 2016; Li, 2019a]. The potential flow theory describes the flow domain by using Laplace equation as the governing equation, without considering the viscous effect. To accurately solve the ship motion response, Cummins [1962] proposed the impulse response theory based on potential flow method and developed a motion model of floating bodies in random waves [Cummins, 1962]. In impulse response theory, wave radiation force is represented by a convolution term, which decreases the calculation efficiency. Therefore, researchers have begun to use state space function to replace impulse response model in order to reduce calculation time [Taghipour, 2008]. With this approach, the state space model uses input, output and state variables to represent the physical system, and the results indicate that the state space model can significantly improve the analysis efficiency [Zhang, 2016].

Several roll stabilization devices have been studied to ensure safe operation of vessels under high sea conditions, including fin, rudder, bilge keels, gyrostabilizer and their associated control systems [Li, 2016; Liu, 2020; Jimoh, 2021]. These devices can also be classified into an internal or an external stabilisation system [Townsend, 2007]. The external system is similar to the control of bilge keel and rudder, in which the anti-rolling fins with a multivariable control approach are designed to reduce roll motion. The device requires strict rudder characteristics and tends to induce great wears, although it can achieve fine anti-rolling performance [Sharif, 1995]. This kind of system does not affect the lightweight of ship too much, but it is vulnerable to damage and ineffective at zero forward speed. The internal system is represented by the gyrostabiliser, which does not increase hydrodynamic resistance and is especially effective at zero forward speed. As the device uses gyro torque, it can be effective regardless of its location in the hull and can be retrofitted on existing vessels. Early gyrostabilisers showed excellent performance, reducing roll by 95% (RMS) at most in some sailing conditions. Despite this excellent performance, some factors limited the widespread application, such as high cost and lack of controls to maintain performance in different sailing conditions. Nowadays, with the advances in materials, mechanical design and control system, multiple gyros can be used to better control the roll motion, and control systems allow condition monitoring and adaptation of the dynamic characteristics to match changing sailing and environmental conditions [Perez, 2009a]. Thus, the gyrostabiliser has been successfully used to stabilize marine vehicles operating on the free surface, greatly reducing the roll motion of the yachts [Takeuchi, 2011]. It can also be used in the wave-energy capture system; the system was proved useful in providing a means to recover wave energy and improving operational effectiveness [Perez, 2009b; Townsend, 2012]. Additionally, experiments on a barge indicate that the gyrostabilizer can reduce roll motion by almost 50% [Palraj, 2020; Palraj, 2021]. Whether used in actual ships or experiments, the gyrostabilizer has maximized efficiency based on existing control algorithms. Therefore, there is still potential for innovation and fundamental research is necessary to develop this potential, obtaining the feasible control algorithms and optimum performance in controlling dynamic systems is desirable, so combining the gyrostabilizer with other control algorithms is necessary to achieve an effective solution for the nonlinear system [Wu, 2018; Tiwari, 2021].

Thanks to the rapid development of the computer technology, various control algorithms have been widely used in engineering applications, including ship motion control. In handing the challenges posed by the wave-induced nonlinear dynamics, many scholars have studied the traditional proportional integrated differential (PID) control method in the past. PID control was widely used in the early ship motion control and had evolved over the past few decades due to its simple architecture and easy adjustment [Wahid, 2012; Tomera, 2017]. However, it is difficult to deal with the nonlinear dynamic caused by the rough waves. Fortunately, many intelligent algorithms have been developed, such as linear quadratic regulator (LQR) and model predictive

control (MPC) algorithms are the two main optimal control methods. LQR feedback mechanism coupled with disturbance feedback has been proposed [Pascoal, 2005], also the LQR control algorithm is applied to reduce the roll motion of cruise ships in regular waves [Lee, 2011]. Control schemes such as LQR and PID may result in higher oscillations when input/rate saturation occurs. In contrast, the MPC method can better consider the delay of the system and is more suitable for nonlinear systems [Sakawa, 1999; Li, 2018], due to its simple formulation and strong optimization capacity, MPC has been increasingly applied in the field of advanced control in engineering, such as offshore platform vibration [Ma, 2022], path following [Sandeepkumar, 2022], autonomous ship avoidance [Zhang, 2022] and dynamic positioning [Li, 2017]. Furthermore, a model utilizing MPC is proposed for vertical motion control of a passenger ship [Kucukdemiral, 2019], also an adaptive strategy for roll motion stabilization is obtained to deal with variation in sailing conditions and sea states [Jimoh, 2021]. The results are proved to be effective and can achieve fast dynamic response with strong robustness. Therefore, the MPC method is a promising approach for solving the challenges posed by wave-induced nonlinear dynamics in ship motion control. In this work, MPC is adopted to obtain the control strategies and transmit them to the gyrostabilizer, allowing the gyrostabilizer's motion to adjust in real-time based on the ship's movement. The contributions are summarized as follows:

- Compared with the previous studies on the roll stabilization equipment [Li, 2016; Liu, 2020; Jimoh, 2021; Pascoal, 2005; Lee, 2011], the proposed approach in this paper focuses on developing a dynamic model for real-time roll motion control using a gyrostabilizer, which can better control the roll motion;
- Compared with the previous studies on the roll control strategy [Perez, 2009a; Wahid, 2012; Tomera, 2017; Palraj, 2020; Palraj, 2021], a novel and realistic motion control strategy based on MPC algorithm is adopted, which can better handle the explicit model and constraints to achieve optimal or sub-optimal performance under various sea conditions;
- Compared with the previous studies on the roll control consideration factors [Townsend, 2012; Townsend, 2014], the wave memory effect is considered in the real-time roll motion control, which considers the delay of the system.

This paper presents a theoretical framework for the combined gyrostabilizer and MPC approach for roll motion stabilization of ships. The main components of the framework include: Firstly, the dynamic model of roll motion control and hydrodynamic response is presented to describe the behaviour of the ship under different sea conditions. Secondly, the comprehensive system of gyrostabilizer and MPC method are introduced, the retardation effect of radiation moment and the hydrodynamic response are validated using roll response amplitude operators (RAOs) with different frequencies. Thirdly, the comparison of the proposed method is carried out by applying it to a certain ship in the literature. Finally, the dynamic model is validated by analyzing the roll control simulation results of DTMB 5415 with both regular and random beam wave conditions, and possible reasons are given. The main objective of this research is to establish an all-encompassing method that combines the gyrostabiliser and MPC control to achieve higher automation without the need for manual intervention, improve ship stability and effectively reduce the lag issue of traditional control methods. Gyrostabilizers can quickly adjust ships to counteract external disturbances and keep them in a stable state, while MPC control can optimize control based on system states and constraints, resulting in more accurate and efficient control. The combined usage of these two technologies can further improve control accuracy and safety performance, leading to more development opportunities in the shipping industry, and potential applications in various marine engineering fields.

2 Principle of gyroscopic-based roll control systems

The gyrostabilizer roll control system is modelled as a feedback system, as depicted in Fig. 1, where ship excitation dynamics represents the response of the vessel to the resultant excitation moments, while the gyrostabilizer dynamics portray the influence of the gyrostabilizer system on the vessel. It is noteworthy that the gyrostabilizer's impact is contingent upon the selected control strategy.

The gyrostabilizer produces a gyroscopic torque that acts in the opposite direction to the roll moment generated by waves on the vessel. The gyrostabiliser contains a high-speed spinning flywheel that is supported by a single gimbal. When the wave forces on the hull induce roll motion, there is an excitation torque that's proportional to the rate of roll. This excitation torque causes a change in angular momentum that results in precession motion of the spinning wheels. The output gyro torque is then obtained from the spin angular velocity and the precession rate. The roll control gyrostabilizer uses this torque to counteract the roll of the hull, which leads to a reduction in rolling motion. The principle of the gyrostabilizer for roll control is illustrated in Fig. 2.

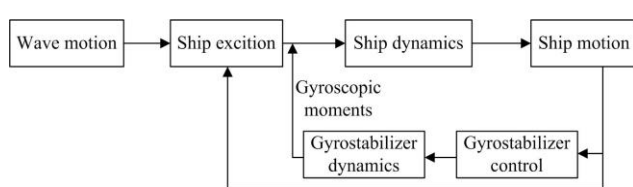


Fig. 1 Diagram for a gyroscopic roll control system.

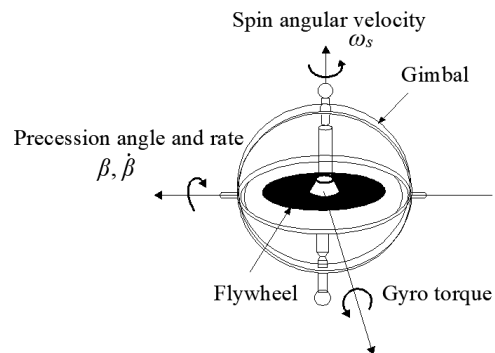


Fig. 2 Operating principle of gyrostabilizer.

The gyrostabiliser can be categorized into passive and active types based on its control mode. In the case of a passive gyrostabiliser, the moment that causes undesirable motion is countered by the gyroscope, resulting in rotation of the gyroscope about its free axis called precession. Hence, the passive gyrostabiliser is of a natural precession type. On the other hand, the active gyrostabiliser system uses a reverse method where the gyroscope rotates around its free axis known as nutation, and the precession of the active gyrostabiliser is driven by the controller. By actively controlling the precession torque, the active gyrostabiliser can provide more accurate controlling performance. Thus, the active gyrostabiliser is utilized for this study.

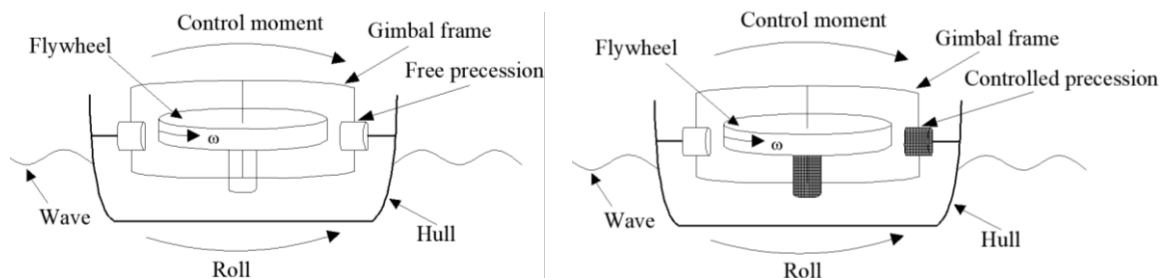


Fig. 3 Sketch of gyrostabiliser system (left) passive control; (right) active control.

As shown in Fig. 3, when used as a stabilization device, regardless of whether the gyrostabiliser is active or passive, using only one gyrostabiliser to generate control moment can cause problems. When the flywheel rotates around its precession axis, the direction of flywheel nutation changes accordingly, resulting in a change in direction of the gyrostabiliser output moment. Thus, the system may generate unexpected moment and lead to

unnecessary yaw or pitch motion of the ship. To solve this issue, dual-flywheel spinning in opposite directions are utilized to prevent the vessel from exciting in the degree of freedom of rotation about the precession axis. This arrangement enables two gyrostabilisers to work together as one group [Townsend, 2007]. The general arrangement of dual gyrostabilisers with ship and their local arrangement are shown in Fig. 4 respectively, which explains the dual gyrostabilisers arrangement along the ship in general, also the local enlarged diagram shows that dual flywheels have equal rotational speed in the opposite direction, and the gyrostabiliser precession speed is equal in the opposite direction. This design ensures that all torque generated in the undesirable direction (pitch and yaw) cancels out, and the output control roll moment doubles.

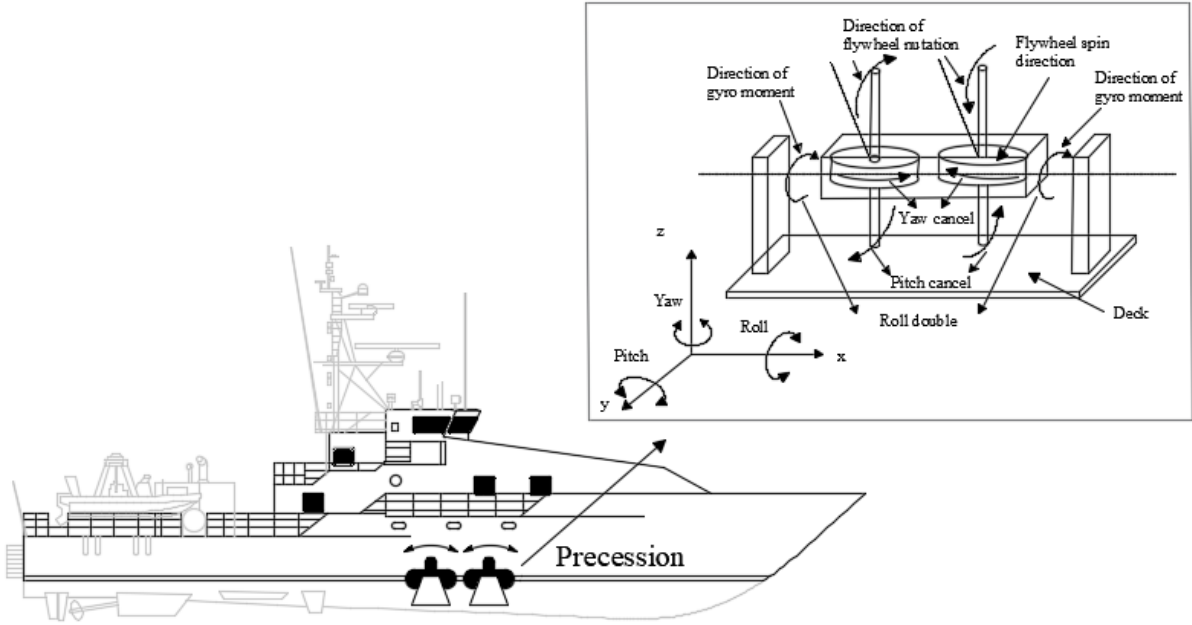


Fig. 4 Arrangement of ship and dual gyrostabilisers.

3 Mathematical model of roll motion

3.1 Dynamic model of roll motion stabilization

According to the impulse response theory [Cummins, 1962], the motion of a marine vessel is typically described using the general model that considers surge, sway, heave, roll, pitch and yaw. However, since the roll motion in beam seas is usually the dominant factor, the six degree-of-freedom (6-DOF) model is often simplified to a one degree-of-freedom (1-DOF) model that only considers the roll motion dynamics. This approach has been adopted in many previous studies [Hinostroza, 2015; Jimoh, 2021]. Therefore, this study will use the 1-DOF model, which can be expressed by the following nonlinear equation:

$$(I_{xx} + J_{xx})\ddot{\phi}(t) + \int_0^t h(t - \tau)\dot{\phi}(\tau)d\tau + K\phi(t) = M_{wave}(t), \quad (1)$$

where I_{xx} is the transverse inertia moment of the ship; J_{xx} is the ship's added mass inertia moment at infinite frequency; $\phi(t)$, $\dot{\phi}(t)$, $\ddot{\phi}(t)$ is the ship's roll angle, roll velocity and roll acceleration, respectively; K is the ship's restoring coefficient of roll moment; $M_{wave}(t)$ is the wave excitation moment; and h is the kernel

function for retardation that represents the memory effect of the free surface, and it is expressed in the time-domain. When considering a gyrostabiliser system that has multiple counter rotating spinning flywheels, the degrees of freedom of flywheels which are related to roll motion of a ship can be isolated in the motion dynamic analysis. With the analysis mentioned above, a roll motion model for a ship along with dual-flywheel gyrostabiliser can be expressed as follows:

$$\begin{aligned} (I_{xx} + J_{xx})\ddot{\phi}(t) + \int_0^t h(t-\tau)\dot{\phi}(\tau)d\tau + K\phi(t) &= M_{wave}(t) - mI_s\omega_s\dot{\beta}(t)\cos\beta(t) \\ I_t\ddot{\beta}(t) + B_g\dot{\beta}(t) + C_g\beta(t) &= I_s\omega_s\dot{\phi}(t)\cos\beta(t) + M_c(t) \end{aligned}, \quad (2)$$

where for the dual-gyrostabiliser setup, $m = 2$; I_s is the polar inertia moment to the reference point; I_t is the inertia of the single spinning flywheel along the precession axis; ω_s is the spin angular velocity, which is assumed as a constant value in this paper; B_g is the damping coefficient associated with the friction; C_g is the restoring coefficient with the mass distribution of the spinning flywheel; $\beta(t)$, $\dot{\beta}(t)$, $\ddot{\beta}(t)$ is the precession angle, precession velocity and precession acceleration; and $M_c(t)$ is the control moment. The first equation in Eq. (2) represents the ship roll dynamics, while the latter one describes the dynamics of the gyro about the precession axis. The control moment $M_c(t)$ is treated as the manipulated variable (MV) in this study, the motion response of ship and gyrostabilizer $\phi(t)$, $\dot{\phi}(t)$, $\beta(t)$, $\dot{\beta}(t)$ are called states.

3.2 Hydrodynamic response

This paper applies the linear potential flow theory, which is the most widely used method, to obtain the hydrodynamic coefficients of the ship. This theory assumes that the fluid is non-rotational, non-viscous and incompressible. With this assumption, the basic equations of fluid mechanics can be greatly simplified [Ma, 2018]. The velocity potential in the flow field can be divided into three parts:

$$\varphi(x, y, z, t) = \varphi_r + \varphi_i + \varphi_d, \quad (3)$$

where $\varphi(x, y, z, t)$ is the velocity potential that describes the flow within the fluid domain, φ_r is the radiation potential generated by the floating body movement, φ_i is the incident potential of waves not disturbed by floating bodies, φ_d is the wave diffraction potential generated after the wave passes through the floating body, and $\mathbf{r} = (x, y, z)$ indicates the position of the ship's centre of gravity. The velocity potential $\varphi(x, y, z, t)$ satisfies the Laplace equation, seabed boundary conditions, free surface conditions and remote radiation conditions in the entire fluid domain. Therefore, its calculation is converted to a boundary value problem. Based on the solution of the velocity potential, the Bernoulli equation is used to obtain the hull pressure, and then the wave moment acting on the hull is solved by integration along length direction of the ship, in which the Froude-Krylov moment and the hydrostatic moment are obtained by directly integrating the pressure on the instantaneous wet surface in the time domain, and the diffraction moment is acquired by integrating on the average wet surface of the hull [Suner, 2022; Bu, 2020]. The wave excitation moment is obtained as follows:

$$M_{wave}(t) = M_{F-K}(t) + M_d(t), \quad (4)$$

where $M_{F-K}(t)$ is the Froude-Krylov (F-K) moment generated by the wave undisturbed by floating bodies; $M_d(t)$ is the diffraction moment generated by the wave passing through the floating body. In the case of beam

waves, $M_{wave}(t)$ is the wave excitation moment based on the Froud–Krylov hypothesis. The sea condition adopted in the paper is the Joint North Sea Wave Project (JONSWAP) wave spectrum, which is considered to be where the majority of marine vessels operate.

4 Model predictive control

4.1 MPC theory

MPC, known as receding horizon control, is a multi-variable control system that has become an attractive feedback strategy and is increasingly being applied in the field of advanced control. MPC has a simple formulation and strong optimization capacity, which enables it to handle the explicit model and constraints [Zhang, 2022]. Its most prominent feature is its ability to consider future time point while optimising the current time point. The flowchart of MPC is shown in Fig. 5. First, the system state x is estimated based on the initial conditions. Then, the optimal input is computed by minimising the cost function over a prediction horizon using the system model [Fossen, 2011]. Finally, the optimal input is implemented, the state of the system is re-evaluated and the optimal control input is fed back to the plant to update the current plant state. In the new receding horizon, the optimization loop is repeated to generate the optimal control input, and the receding process continues until the end of the time horizon. The entire procedure, which involves repeated prediction and optimization, aims to find a new input with the control and prediction horizons moving forward. The calculation of the applied input based on the predicted system behaviour allows for the inclusion of state constraints and input as well as the optimization of the given cost function [Findeisen, 2002]. The nonlinear MPC method can make more accurate decisions because it solves an open-loop constrained optimization problem given the current plant states with the availability of a nonlinear dynamic model. Therefore, it is an ideal tool for solving problems such as ship roll motion control.

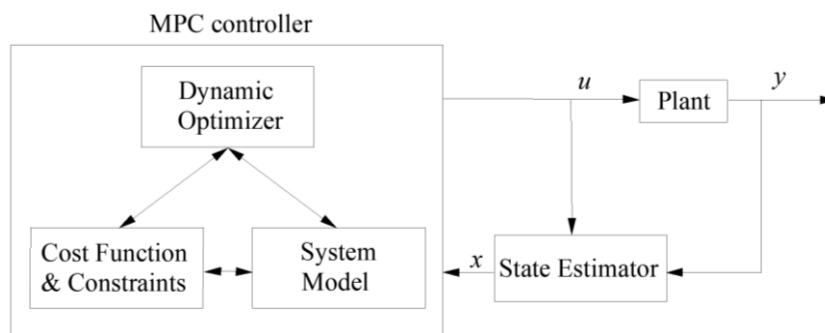


Fig. 5 Closed loop control of MPC method.

This study originally applies the nonlinear MPC method to control ship motion in regular and irregular waves, where state space representative and cost function are the most important parts in MPC. The MPC controller is implemented through the MATLAB Model Predictive Controller Toolbox. The cost function, state space, and other parameters can be customized by the user, while the dynamic optimizer module is set as the default. All the computations are performed on a 16-core (Intel Xeon, 2.4 GHz) server computer.

4.2 State space representative

4.2.1 Representative of memory effect

In Eq. (1) and Eq. (2), the integral form of radiation moment makes it inconvenient to implement the control strategy. Therefore, an alternative model has been developed to account for the memory effect of the free surface. In this model, the radiation moment is expressed using a state-space model [Perez, 2009c]. The frequency domain identification methods are used with greater accuracy since the transfer function of the correct relative degree can be chosen before the identification process. This is just a brief introduction to the principle.

We denote a system with roll velocity $\dot{\phi}$ as the input and radiation moment $y(t)$ as the output, the following approaches are available to represent the dynamic process. Here, Eq. (5) is the ordinary differential equation of order n , while Eq. (6) is its convolution integral expression, and Eq. (7) represents it in its state-space form. These three formulas Eq. (5)-(7) can be equivalent to each other. When transforming Eq. (5) into state-space form using Eq. (7), the matrices shown in Eq. (8) are obtained.

$$\frac{d^n y}{dt^n} + q_{n-1} \frac{d^{n-1} y}{dt^{n-1}} + \dots + q_1 \frac{dy}{dt} + q_0 y = p_{n-1} \frac{d^{n-1} \dot{\phi}}{dt^{n-1}} + p_{n-2} \frac{d^{n-2} \dot{\phi}}{dt^{n-2}} + \dots + p_1 \frac{d\dot{\phi}}{dt} + p_0 \dot{\phi}. \quad (5)$$

$$y(t) = \int_0^t h(t-\tau) \dot{\phi}(\tau) d\tau. \quad (6)$$

$$\begin{aligned} \dot{\mathbf{u}}(t) &= \vec{\mathbf{A}} \cdot \vec{\mathbf{u}}(t) + \vec{\mathbf{B}} \cdot \dot{\phi}(t) \\ y(t) &= \vec{\mathbf{C}} \cdot \vec{\mathbf{u}}(t) + \vec{\mathbf{D}} \cdot \dot{\phi}(t) \end{aligned} \quad (7)$$

$$\vec{\mathbf{A}} = \begin{bmatrix} -q_{n-1} & -q_{n-2} & \dots & -q_1 & -q_0 \\ 1 & 0 & \dots & 0 & 0 \\ 0 & 1 & \dots & 0 & 0 \\ \vdots & \vdots & \ddots & 0 & 0 \\ 0 & 0 & \dots & 1 & 0 \end{bmatrix} \in R^{n \times n}, \quad \vec{\mathbf{B}} = \begin{bmatrix} 1 \\ 0 \\ 0 \\ \vdots \\ 0 \end{bmatrix} \in R^{n \times 1}, \quad (8)$$

$$\vec{\mathbf{C}} = [p_{n-1} \quad p_{n-2} \quad \dots \quad p_1 \quad p_0] \in R^{1 \times n}$$

where $\vec{\mathbf{u}}(t) \in R^{n \times 1}$ is the state vector of ordinary differential equation in Eq. (7); $\vec{\mathbf{A}}$, $\vec{\mathbf{B}}$, $\vec{\mathbf{C}}$ are the state-space model that transfer function can convert with $\vec{\mathbf{D}} = \mathbf{0}$ directly. The time-domain expression of h in Eq. (2) can be obtained either from the added mass $J_{xx}(\omega)$ or the potential damping $B(\omega)$ in the frequency domain shown in Eq. (9), which is able to transform to the frequency domain through the Fourier transformation by Eq. (10), then the transfer function is established to approximate $h(i\omega)$ with Eq. (11). To obtain the parameters p and q , least squares method is adopted to estimate the coefficient matrices [Li, 2019b]. The estimation of $\vec{\mathbf{A}}$, $\vec{\mathbf{B}}$, $\vec{\mathbf{C}}$ is solved based on the system identification [Taghipour, 2008].

$$h(t) = \frac{2}{\pi} \int_0^\infty \frac{J_{xx}(\omega)}{\omega} \sin(\omega t) d\omega = \frac{2}{\pi} \int_0^\infty B(\omega) \cos(\omega t) d\omega. \quad (9)$$

$$h(i\omega) = \int_0^\infty h(\tau) e^{-i\omega\tau} d\tau = B(\omega) + i\omega [J_{xx}(\omega) - J_{xx}]. \quad (10)$$

$$\hat{h}(i\omega, p, q) = \frac{p_{n-1}(i\omega)^{n-1} + p_{n-2}(i\omega)^{n-2} + \dots + p_0}{(i\omega)^n + q_{n-1}(i\omega)^{n-1} + \dots + q_0}. \quad (11)$$

4.2.2 State-space representative of the plant

Considering that states, memory effects and MV are coupled in a dynamic model, the state-space representation can be expressed as

$$\begin{aligned} (I_{xx} + J_{xx})\ddot{\phi}(t) + \bar{C}\ddot{u}(t) + K\phi(t) &= M_{wave}(t) - mI_s\omega_s\dot{\beta}(t)\cos\beta(t) \\ I_r\ddot{\beta}(t) + B_g\dot{\beta}(t) + C_g\beta(t) &= I_s\omega_s\dot{\phi}(t)\cos\beta(t) + M_c(t) \\ \dot{u}(t) &= \bar{A}\cdot\bar{u}(t) + \bar{B}\cdot\dot{\phi}(t) \end{aligned}, \quad (12)$$

A state vector is defined $\mathbf{x}(t) = [\phi(t), \dot{\phi}(t), \beta(t), \dot{\beta}(t), \bar{u}(t)^T]^T \in R^{(n+4) \times 1}$. Then, Eq. (12) can be rewritten as

$$\dot{\mathbf{x}}(t) = \gamma \cdot \mathbf{x}(t) + \eta(t)$$

$$\gamma = \begin{bmatrix} 0 & 1 & 0 & 0 & \mathbf{0} \\ -\frac{K}{I_{xx} + J_{xx}} & 0 & 0 & -\frac{2I_s\omega_s}{I_{xx} + J_{xx}} & \bar{B} \\ 0 & 0 & 0 & 1 & \mathbf{0} \\ 0 & \frac{I_s\omega_s}{I_r} & -\frac{C_g}{I_r} & -\frac{B_g}{I_r} & \mathbf{0} \\ \mathbf{0} & \bar{C} & \mathbf{0} & \mathbf{0} & \bar{A} \end{bmatrix}, \quad \eta(t) = \begin{bmatrix} 0 \\ \frac{M_{wave}(t)}{I_{xx} + J_{xx}} \\ 0 \\ \frac{M_c}{I_r} \\ \mathbf{0} \end{bmatrix}. \quad (13)$$

Eq. (13) is a first-order differential equation and serves as an analytical Jacobian matrix for the prediction model. Utilizing this form can significantly improve simulation efficiency and simplify implementation of the control algorithm. To solve Eq. (13), initial conditions are required and a fourth-order Runge–Kutta method is used with the frequency system identification order being $n=4$. Considering the memory effect of radiation moment, this paper simulates the motion control operation using eight states and one MV.

4.3 Cost function and constraints

The cost function and constraints are crucial for the MPC controller, as shown in Fig. 5. The MPC problem is solved over a finite horizon by treating it as a deterministic optimal control problem using the current state as initial conditions. The solution is then implemented in a receding horizon manner. The objective of MPC controller is to minimize the cost function. In motion control problem, a nonlinear cost function J_c in this case is typically used to find the minimal roll angle, subject to certain constraints as indicated in Eq. (15).

$$J_c = \min \sum_{i=0}^N \phi_i^2. \quad (14)$$

Constraints applied at this stage are defined as follows:

$$\begin{aligned} \dot{\mathbf{x}}(t) &= \gamma \cdot \mathbf{x}(t) + \eta(t) \\ \mathbf{x}(t) &\in [x_l, x_u] \\ \mathbf{x}(0) &= \mathbf{x}_{initial} \end{aligned}. \quad (15)$$

The first constraint in Eq. (15) represent the state space of the ship and gyrostabilizer's hydrodynamic; while the second constraint pertains to the boundary condition of the states. The subscripts l and u indicate the

lower and upper bounds, respectively. The final constraint represents the initial condition of the roll motion control equation. The standard deviation s of the roll angle is defined as follows:

$$s = \sqrt{\frac{1}{N} \sum_{i=1}^N (\phi_i - \mu)^2}, \quad (16)$$

$$r = (s_n - s_c) / s_n \times 100\%$$

where μ is the average of roll angle, ϕ_i is the roll angle at i -th time step, r is the roll reduction rate, s_n is the roll angle standard deviation without control, and s_c is the roll angle standard deviation after control.

5 Simulation result

This paper utilizes the standard ship model DTMB 5415 for analysis, the hydrodynamic coefficients as K , $J_{xx}(\omega)$ and $B(\omega)$ are solved using the AQWA software [Gao, 2017], which is based on the potential theory, and successfully used to analyse the wave motion of ship, wave load on fixed structure and et al with high accuracy. Also, the AQWA result is regarded as the reference for comparison with the simulation model. The hydrodynamic model of the ship hull is depicted in Fig. 6. Table 1 and Table 2 display the main data for the DTMB 5415 and gyrostabiliser, respectively. The gyrostabiliser's parameters are obtained according to the ship's main dimensions and related stability data.

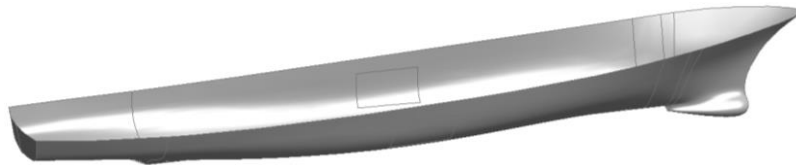


Fig. 6 Hydrodynamic model of ship.

Table 1 Main data of DTMB 5415

Particulars	Value
Length of all (L_{oa}) (m)	153.300
Length of perpendicular (L_{pp}) (m)	142.200
Breath of waterline (B_{wl}) (m)	19.074
Depth (D) (m)	12.470
Draft (T) (m)	6.150
Displacement (Δ) (m^3)	8424
Metacentric height (GM) (m)	1.938
Centre of gravity above base line (KG) (m)	7.555
Roll radius of gyration (k_{xx} -water) (m)	6.932
Pitch and yaw radius of gyration (k_{yy} -air) (m)	0.25L

Table 2 Main data of the gyrostabiliser

Particulars	Value
Transverse inertia moment I_y ($t \cdot m^2$)	20000
Polar inertia moment I_x ($t \cdot m^2$)	40000

Damping B_g ($t \cdot m^2/s$)	50422.81
Restoring moment C_g ($t \cdot m^2/s^2$)	435.03
Speed of revolution ω_s (rpm)	400
Mass (t)	53

5.1 System identification

To ensure the reliability of the obtained state matrices, a comparison is made between the original hydrodynamic coefficients and those estimated by the state matrices, as shown in Fig. 7. The red dot curve represents the original hydrodynamic coefficients based on potential theory, while the blue solid curve indicates the estimated values from system identification. Fig. 7 (left) displays the added mass $J_{xx}(\omega)$ and Fig. 7 (right) shows the potential damping $B(\omega)$. The comparison reveals that the fourth-order state-space model can effectively approximate the convolution term (fluid memory effect), suggesting that the parameters utilized in the state-space are reliable.

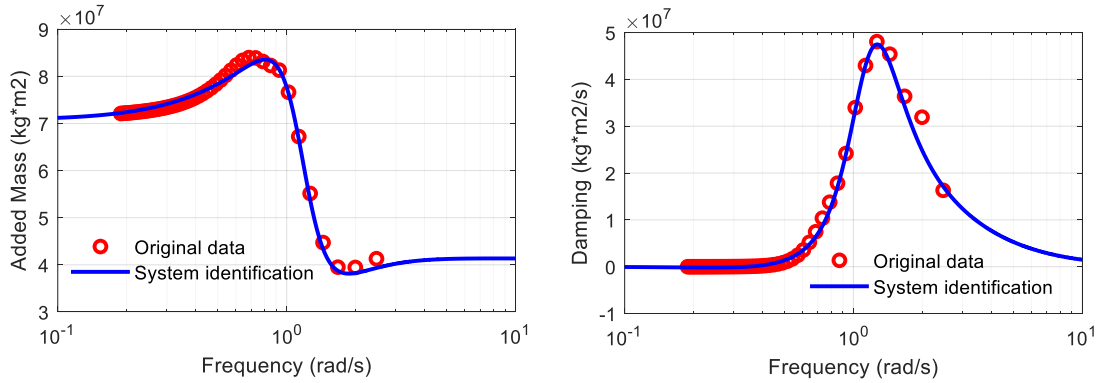


Fig. 7 System identification results of wave memory effect in roll direction (left) added mass; (right) roll damping.

5.2 Validation of hydrodynamic model

To avoid the influence of hull's natural frequency, a regular wave with a wave frequency of $\omega=1.227$ rad/s is selected for the analysis, which is twice the natural frequency of the hull with a wave steepness $\delta=0.02$. Fig. 8 compares the roll frequency response function calculated by AQWA with experiment data [Begovic, 2013], where φ is the roll angle, k is the wave number, A is the wave amplitude, ω is the wave frequency, L is the ship length, and g represents the acceleration due to gravity. Despite some differences between the AQWA result and experiment, the tendency conforms with the experimental data, particularly the peak response, validating the calculation outcome qualitatively.

Due to the ship's large motion amplitude in regular beam wave, its natural frequency is utilized as the wave frequency for analysis. The resulting roll motion response of the ship, including roll angle, roll velocity and roll acceleration, is depicted by the red dash curve in Fig. 9. To validate the model and parameters utilized in this study, the comparison between AQWA software and explicit model is shown in Fig. 9, where the control moment $M_c(t)$ in Eq. (12) and Eq. (13) is considered zero, thus simulating a scenario where the gyrostabilizer ceases to work. This simulation equates to a 1-DOF ship motion and represented by the black dot curve in Fig. 9. The comparison shows that there is minimal discrepancy between the two results, with a maximum error of only

5%. This further illustrates the reliability of the identification system and the parameters used. When integrated with the parameters of the ship and gyrostabiliser, the system identification produces results similar to those obtained from the simulation.

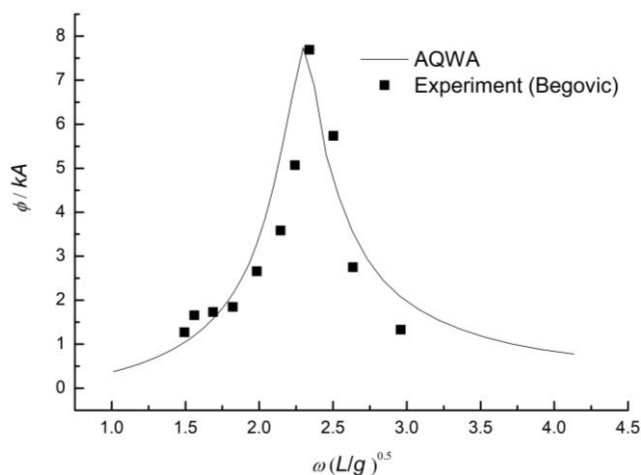


Fig. 8 Result comparison of roll frequency response.

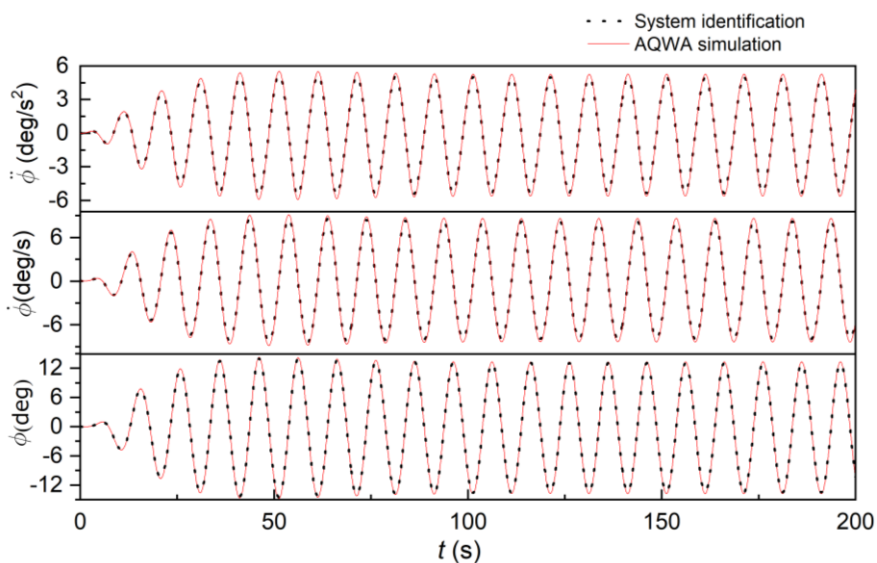


Fig. 9 Roll motion response result (regular wave, $\omega=1.227$ rad/s; $\delta=0.02$).

5.3 Comparison of MPC and gyrostabilizer control with the literature

To validate the proposed MPC with gyrostabilizer control method, the performance of a certain ship under random sea waves is investigated and compared with the existing literature using the same experimental conditions [Liu, 2022]. The active controlled gyrostabilizer is used to stabilize the rolling motion via MATLAB Simulink in the literature. A JONSWAP spectrum is adopted for the wave power spectrum, and a wave moment for a significant wave height of 2m is generated, which is shown in Fig. 10. The control time for MPC method in the study is 50s, and the historical wave moment curve between 100s-150s is used as the control target. The control moment generated by the combined MPC and gyrostabilizer method is depicted in Fig. 11, while the

comparison of wave moment $M_{wave}(t)$ and gyrostabilizer moment $mI_s\omega_s\dot{\beta}(t)\cos\beta(t)$ in the roll direction is shown in Fig. 12. It can be observed that both wave moment and gyrostabilizer moment have similar tendencies, with nearly equal magnitudes but opposite directions. As a result, they reduce the roll response magnitude to a very small range. Fig. 13 depicts active control activities for control methods considered. The solid black curve represents the active control only by gyrostabilizer [Liu, 2022], while the dash-dot red curve represents the combined MPC and gyrostabilizer method proposed in this paper. Table 3 compares the roll angle result within these two methods. It can be also observed that the maximum roll angle magnitude decreases from 14.523deg to 1.610deg and 0.303deg respectively after active control, indicating a noticeable reduction in the roll magnitude. The roll angle standard deviation also changes from 7.244deg to 0.780deg and 0.073deg, showing the effectiveness of the proposed MPC with gyrostabilizer method in controlling the ship roll motion to a better degree compared to only using gyrostabilizer. Accordingly, the proposed method in the paper requires a larger range of precession angle, the maximum precession angle magnitude is 32deg, which is larger than 22deg of gyrostabilizer control, as shown in Fig. 14.

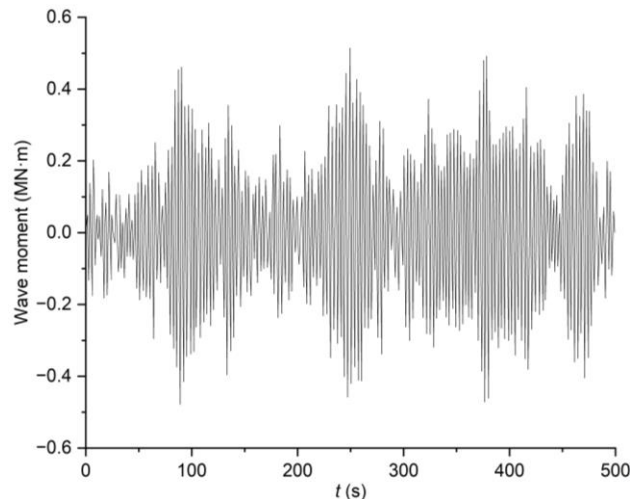


Fig. 10 Wave moment used for comparison (irregular wave, $H_s=2m$).

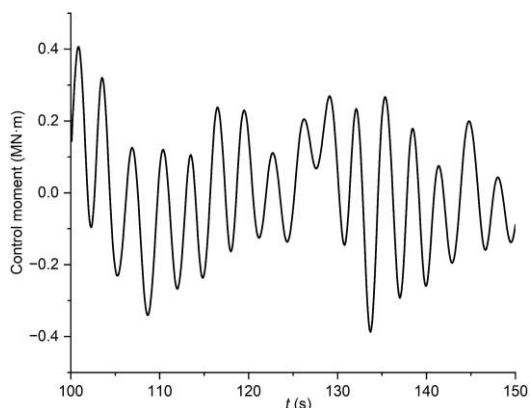


Fig. 11 Control moment by MPC method.

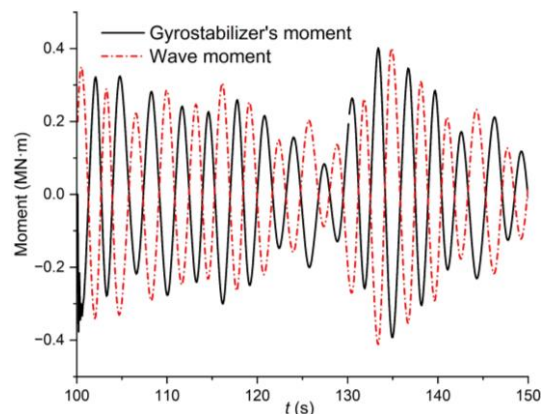


Fig. 12 Wave moment and gyrostabiliser moment.

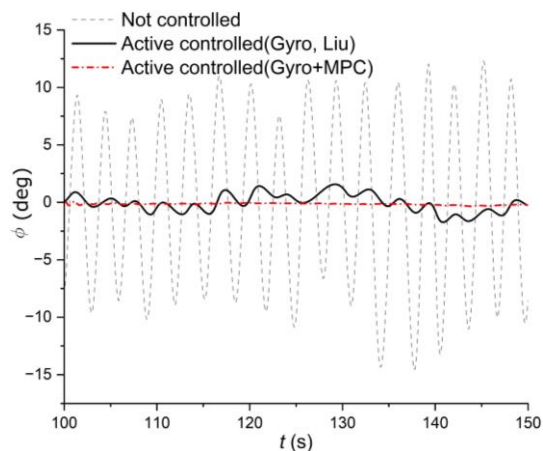


Fig. 13 Roll motion result comparison.

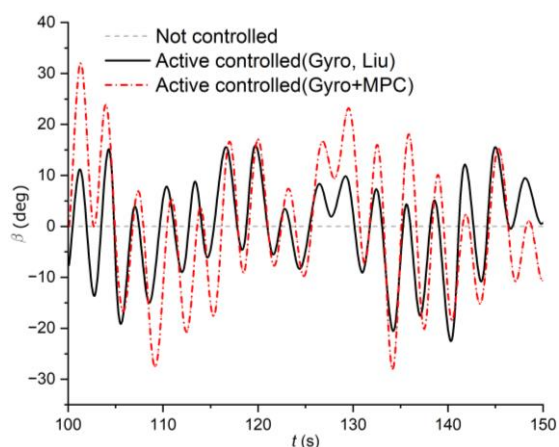


Fig. 14 Precession motion result comparison.

Table 3 Roll angle comparison with the literature

Particulars	Without control	Gyrostabilizer	MPC+gyrostabilizer
Maximum roll angle magnitude (deg)	14.523	1.610	0.303
Mean roll angle (deg)	-0.196	-0.050	-0.148
Roll angle standard deviation (deg)	7.244	0.780	0.073

5.4 Case study with regular wave

Based on the comparison with the literature, a study is carried out to validate the effectiveness of the proposed MPC and gyrostabilizer method on the nonlinear dynamic model of the ship roll motion, with the goal of reducing the motion response of the ship in regular beam wave conditions of the wave frequency $\omega=0.614$ rad/s and wave steepness $\delta=0.02$. The numerical simulation utilizes an active gyrostabilizer to generate roll moment via precession, by means of adjusting the precession angle and velocity to meet control requirements. The output vector of the control moment is shown in Fig. 15. Fig. 16 displays the wave moment and the gyrostabiliser's moment in the roll direction, which indicates that the gyrostabiliser's moment in the roll direction is equal in magnitude and opposite in direction to the input vector of wave moment. The MPC method is used to generate the control input based on wave moment, and the optimal solution is determined through the cost function, constraints and current wave condition. This ensures that the gyrostabiliser moment in the roll direction opposes the wave moment throughout the entire time duration. The results indicate that the optimization process finds the optimal solution for the current condition, resulting in remarkably small roll motion, and the parameters adopted in the study are deemed reasonable.

The roll motion response and gyrostabiliser parameters during the control process are displayed in Fig. 17. It can be observed that the control greatly reduced the roll angle and velocity. The precession angle and precession velocity of the gyrostabiliser follow a periodic pattern in response to the regular wave conditions, with the precession angle changing from approximately -5deg to 5deg, and the precession velocity ranging from around -4deg/s to 4deg/s. However, due to the memory effect of radiation moment consideration in the roll motion equation, the initial control stage of roll angle and velocity exhibit non-periodic phenomena. With state-space representation, the proposed method significantly increases computation speed, enabling the optimal strategy to be found within 15min for 50s of control time. Comparing with the roll angle of active control and

the initial condition without control, as shown in Fig. 18, the maximum roll angle magnitude decreases from 14.593deg to 0.393deg, while the roll angle standard deviation changes from 7.659deg to 0.22deg, just depicted as the regular wave in Table 4. Overall, the roll motion is reduced by 97.01%, demonstrating that the combination of MPC with the gyrostabiliser method can effectively control the ship motion.

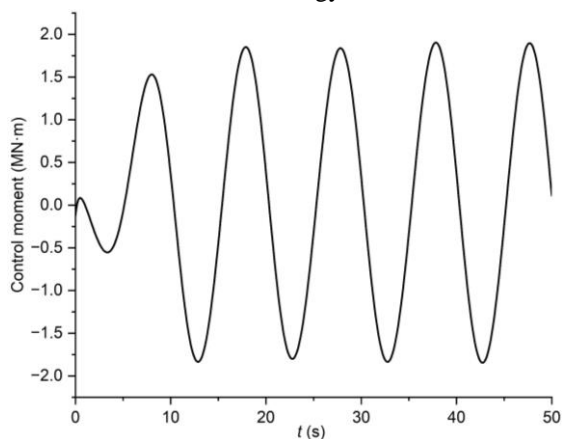


Fig. 15 Control moment by MPC method ($\omega=0.614$ rad/s).

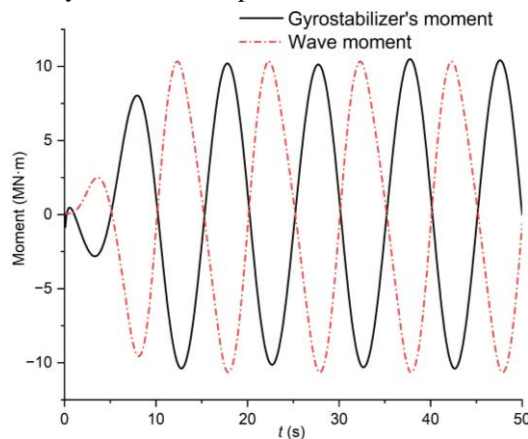


Fig. 16 Wave moment and gyrostabiliser moment.

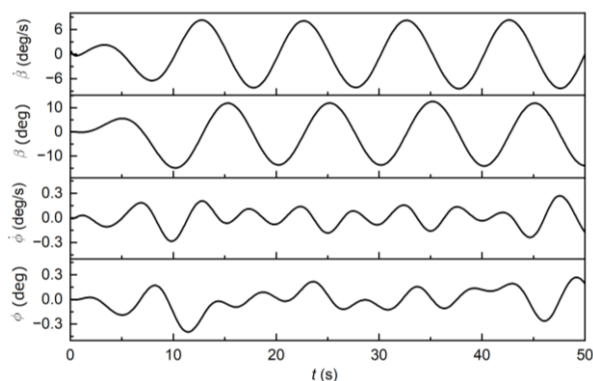


Fig. 17 Roll motion response and parameters of gyrostabiliser.

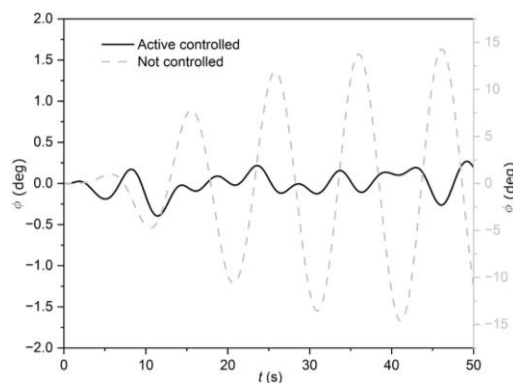


Fig. 18 Roll angle comparison between active control and without control (regular wave).

5.5 Case study with random wave

The model of wave induced moment can be described by a stochastic process based on JONSWAP spectrum. The simulation of the ship model is performed under rough sea conditions with significant wave height of 6 m, the peak frequency ω_p of 0.885 rad/s and the spectral peak factor of 1. Fig. 19 shows the time domain roll motion response of the ship under beam waves and compares the numerical simulation results with those obtained from system identification. The control moment obtained by the MPC method is displayed in Fig. 20. Fig. 21 demonstrates that the input vector of wave moment and the gyrostabiliser's moment in the roll direction have almost equal magnitude but opposite direction. The roll motion response between 100s and 150s, shown in the blue box in Fig. 19, is selected for the analysis due to its larger amplitude. Fig. 22 displays the ship's roll motion response and gyrostabiliser parameter during the 50s control process, revealing that the precession angle and precession velocity of the gyrostabiliser change with the wave moment. Irregular wave conditions result in irregular motion responses of the ship and the gyrostabilizer's precession. During the 50s

control process, the maximum roll angle amplitude changes from 12.727deg to 0.254deg, the roll angle standard deviation decreases from 5.398deg to 0.110deg, just shown in Table 4, the roll motion is reduced by almost 97.84%, indicating a significant decrease in roll motion. Fig. 23 displays the roll angle with active control, as well as the initial condition without control. The motion control effect with an irregular wave is similar to that of the regular wave, the proposed MPC and gyrostabilizer method offer a preferable control strategy under irregular wave conditions. Overall, the study demonstrates that the MPC and gyrostabilizer method can significantly reduce the roll motion of ships according to the current system parameters, whether under regular or irregular wave conditions.

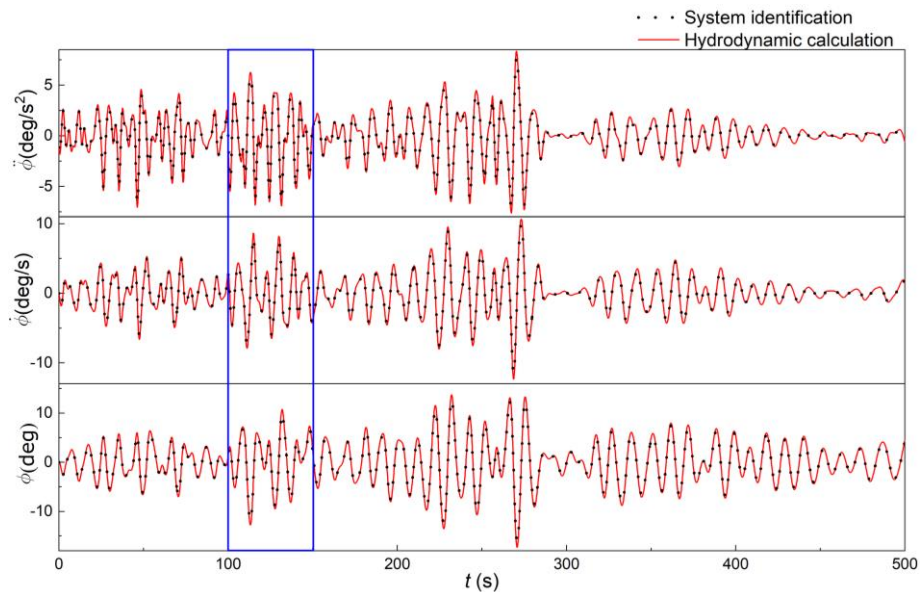


Fig. 19 Roll motion response (irregular wave, $H_s=6m$, $\omega_p=0.885$ rad/s).

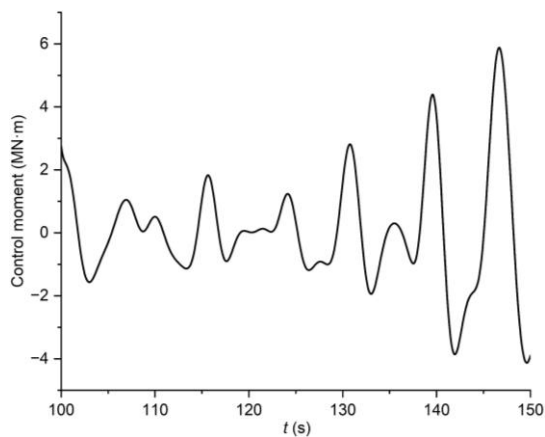


Fig. 20 Control moment by MPC method.

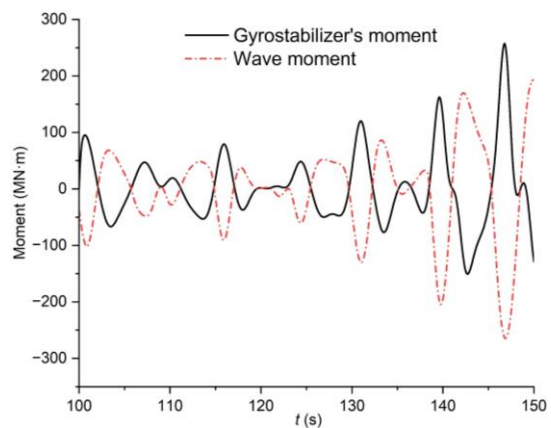


Fig. 21 Wave moment and gyrostabiliser's moment.

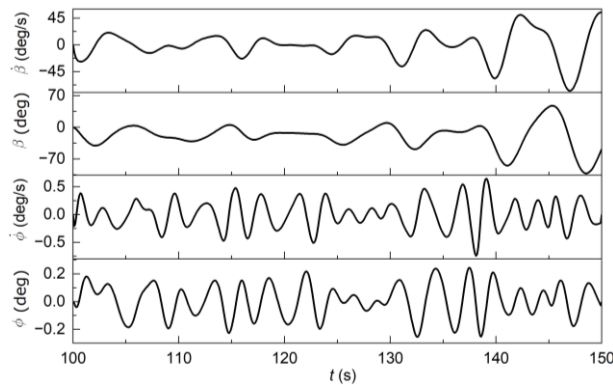


Fig. 22 Roll motion response and parameters of gyrostabiliser.

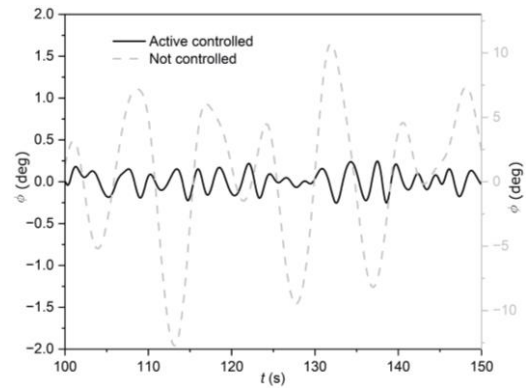


Fig. 23 Roll angle comparison between active control and without control.

Table 4 Roll angle result comparison with regular and irregular wave

Condition	Particulars	Without control	MPC+gyrostabilizer
Regular wave	Maximum roll angle magnitude (deg)	14.593	0.393
	Mean roll angle (deg)	-0.020	-0.022
	Roll angle standard deviation (deg)	7.659	0.220
Irregular wave	Maximum roll angle magnitude (deg)	12.727	0.254
	Mean roll angle (deg)	0.447	0.007
	Roll angle standard deviation (deg)	5.398	0.110

6 Conclusions

This study has proposed a novel roll motion control algorithm that combines the MPC and gyrostabilizer. By using a nonlinear dynamic model, this method can provide more accurate strategies than traditional methods and is particularly suitable for nonlinear systems. The method considers the retardation effect of waves in the state-space representation, making it easier to implement and increasing computational speed. The computed optimal control is used in every time step to ensure that the system is driven according to the minimisation of the cost function. The RAOs between the numerical analysis and experiment are compared, and the nonlinear dynamic model of MPC and gyrostabilizer system without control is validated. Furthermore, the proposed method is analyzed and compared with certain ship motion control methods in the literature. Also the roll motion stabilization of standard ship model is accomplished with regular and random wave conditions respectively. The results indicate that the MPC and active gyrostabilizer combination control method show a significant reduction in roll motions and control the ship roll motion better than only the gyrostabilizer method. This could be a useful guidance for the roll motion control with severe wave conditions and offer a feasible research methodology in the ship motion control domain.

In this paper, the study mainly focuses on the theoretical model analysis without considering some system dissipation factors that may affect the control efficiency in the real ship. Further research exploring the performance of combined system exerted in a real ship will be carried out. Additionally, wave moment is supposed to be known in advance in the study, but it is unknown in real ship, so the prediction of future wave moment has become an important aspect for real-time control, which will be realized using artificial neural

network in the next step. The analysis mentioned above aimed to address 1-DOF roll motion control, it would also be interesting to analyze the performance of the control method when coupling the ship roll motion with other direction of motions (pitch, heave) under an irregular beam wave, and related experimental research and analysis with a random wave direction will be conducted in the next step.

Declaration of competing interest

The authors declare that they have no known competing financial interests or personal relationships that could have appeared to influence the work reported in this paper.

CRedit authorship contribution statement

Lifen Hu: Conceptualisation, Methodology, Software, Investigation, Data curation, Writing - original draft, review & editing. **Ming Zhang:** Software, Data curation, Writing - review & editing. **Xingxing Yu:** Investigation, Methodology. **Zhiming Yuan:** Investigation, Writing - review & editing. **Wubin Li:** Software, Writing - review & editing.

Acknowledgments

This study was supported financially by the Natural Science Foundation of Shandong Province (Grant No. ZR2020ME263, ZR2019PA008); the Open Project Program of Shandong Marine Aerospace Equipment Technological Innovation Center, Ludong University (Grant No. MAETIC2021-10); China Scholarship Council Foundation (CSC201806680085), the National Natural Science Foundation of China (Grant Nos. 51979131, 51509124 and 51681340360). The authors extend their sincere gratitude to the abovementioned organizations.

References

- Begovic, E., Mortola, G., Incecik, A., Day, A. H., 2013. Experimental assessment of intact and damaged ship motions in head, beam and quartering seas. *Ocean Engineering*, 72, 209-226.
- Bu, S., Gu, M., 2020. Unified viscous and potential prediction method for the coupled motion of damaged ship and floodwater in calm water. *Ocean Engineering*, 210, 107441.
- Cummins, W., 1962. The impulse response function and ship motions. *Schiffstechnik*, 9, 101-109.
- Fossen, T., *Handbook of Marine Craft Hydrodynamics and Motion Control*. Norway: John Wiley & Sons Ltd, 2011.
- Findeisen, R., Allgöwer, F., 2002. An introduction to nonlinear model predictive control, 21st Benelux Meeting on Systems and Control, The Netherlands: 119–141.
- Gao, W, Dong, L, Huang, J., *ANSYS AQWA Software introduction and improvement*. China: China WaterPower Press, 2017.
- Gao, Z., Wang, Y., Su, Y., 2020. On damaged ship motion and capsizing in beam waves due to sudden water ingress using the RANS method. *Applied Ocean Research*, 95, 102047.
- Hinojosa, M., Luo, W., Soares, C.G., 2015. Robust fin control for ship roll stabilization based on l2-gain design. *Ocean Engineering*, 94, 126–131.

- Hu, L., Wu, H., Yuan, Z., Li, W., Wang, X., 2021. Roll motion response analysis of damaged ships in beam waves. *Ocean Engineering*, 227, 108558.
- Irkal, M., Nallayarasu, S., Bhattacharyya, S., 2019. Numerical prediction of roll damping of ships with and without bilge keel. *Ocean Engineering*, 179, 226–245.
- Jimoh, I. A., Küçükdemiral, I. B., Bevan, G., 2021. Fin control for ship roll motion stabilisation based on observer enhanced MPC with disturbance rate compensation, *Ocean Engineering*, 224, 108706.
- Kang, H., Yang, Y., Choi, J., Lee, Jong., Lee, Dong., 2013. Time basis ship safety assessment model for a novel ship design. *Ocean Engineering*, 59, 179-189.
- Kucukdemiral, I., Cakici, F., Yazici, H., 2019. A model predictive vertical motion control of a passenger ship, *Ocean Engineering*, 186, 106100.
- Lee, S., Rhee, K., Choi, J., 2011. Design of the roll stabilization controller, using fin stabilizers and pod propellers. *Applied Ocean Research*, 33(4), 229-239.
- Li, Y., Zhu, R., Miao, G., Fan, J., 2016. Numerical method of ship motions coupled with tank sloshing based on fully time domain potential flow theory. *Journal of Ship Mechanics*, 20(11), 1369-1380.
- Li, R., Li, T., Bai, W., Du, X., 2016. An adaptive neural network approach for ship roll stabilization via fin control. *Neurocomputing*, 173, 953–957.
- Li, W., Sun, Y., Chen, H., Wang, G., 2017. Model predictive controller design for ship dynamic positioning system based on state-space equations. *Journal of Marine Science and Technology*, 22, 426-431.
- Li, L., The development of a realtime wave energy device control algorithm based on artificial neural network. Scotland: University of Strathclyde, 2018.
- Li, L., Liu, Y., Yuan, Z., Gao, Y., 2019. Dynamic and structural performances of offshore floating wind turbines in turbulent wind flow. *Ocean Engineering*, 179, 92-103.
- Li, L., Gao, Z., Yuan, Z., 2019. On the sensitivity and uncertainty of wave energy conversion with an artificial neural-network-based controller. *Ocean Engineering*, 183, 282-293.
- Liu, C., Wang, D., Zhang, Y., Meng, X., 2020. Model predictive control for path following and roll stabilization of marine vessels based on neurodynamic optimization. *Ocean Engineering*, 217, 107524.
- Liu, Y., Xia Z., Tang Y., Zhang J., Fan S., 2022. Research on the ship roll stabilization with gyrostabilizer. *Proceedings of the 3rd National Conference on Stability of Ships*, 211-215, Shanghai, China.
- Ma, C., Zhu. Yi., He. J., Zhang. C., Wan. D., Yang. C., Noblesse. F., 2018. Nonlinear corrections of linear potential-flow theory of ship waves. *European Journal of Mechanics - B/Fluids*, 67, 1-14.
- Ma, H., Zhang, Y., Wang, S., Xu, J., Su, H., 2022. Rolling-optimized model predictive vibration controller for offshore platforms subjected to random waves and winds under uncertain sensing delay, *Ocean Engineering*, 252, 111054.
- Palraj, M., Rajamanickam, P., 2021. Motion control studies of a barge mounted offshore dynamic wind turbine using gyrostabilizer. *Ocean Engineering*, 237, 109578.
- Pascoal, R., Rodrigues, B., Soares, C.G., 2005. Roll-yaw regulation using stabilizing fins and rudder in a disturbance observer based compensator scheme. *Maritime Transportation and Exploitation of Ocean and Coastal Resources*, Two Volume Set. CRC Press, pp. 740–747.
- Palraj, M., Rajamanickam, P., 2020. Motion control of a barge for offshore wind turbine (OWT) using gyrostabilizer. *Ocean Engineering*, 209, 107500.

- Perez, T., Steinmann, P. D., 2009a. Analysis of Ship Roll Gyrostabiliser Control. Proceedings of the 8th IFAC International Conference on Manoeuvring and Control of Marine Craft, 310-315, Guarujá Brazil.
- Perez, T., Santos-mujica, M., Ruiz-minguela, J., 2009b. Performance analysis and control design of a gyro-based wave energy converter. Proceeding of European Control Conference, 3743-3748, Budapest, Hungary.
- Perez, T., Fossen, T., 2009c. A Matlab Toolbox for Parametric Identification of Radiation-Force Models of Ships and Offshore Structures. Modeling, Identification and Control, 30(1), 1-15.
- Ruth, E., Olufsen, O., Rognebakke, O., 2019. CFD in damage stability, Proceedings of the 17th International Ship Stability Workshop, 259-263, Helsinki, Finland.
- Sakawa, Y., 1999. Trajectory Planning of A Free-flying Robot by Using the Optimal Control. Optimal Control Applications & Methods, 20, 235-248.
- Sandeepkumar, R., Rajendran, S., Mohan, R., Pascol, A., 2022. A unified ship manoeuvring model with a nonlinear model predictive controller for path following in regular waves, Ocean Engineering, 243, 110165.
- Sharif, M., Roberts, G., Sutton, R., 1995. Sea-trial experimental results of fin/rudder roll stabilisation. Control Engineering Practice, 3(5), 703–708.
- Suner, M., Bas, M., 2022. A new approach to narrow waterways traffic routing with potential flow theory and CFD. Ocean Engineering, 261, 111862.
- Taghipour, R., Perez, T., Moan, T., 2008. Hybrid frequency-time domain models for dynamic response analysis of marine structures. Ocean Engineering, 35(7), 685-705.
- Takeuchi, H., Umemura, K., Maeda, S., 2011. Development of the anti rolling gyro 375T (rolling stabilizer for yachts) using space control technology. Mitsubishi Heavy Industries Technical Review. 48(4), 70–75.
- Tiwari, K., Krishnankutty, P., 2021. Dynamic positioning of an oceanographic research vessel using fuzzy logic controller in different sea states. Marine Systems & Ocean Technology, 16, 221–236.
- Townsend, N., Murphy, A., Sheno, R., 2007. A new active gyrostabilizer system for ride control of marine vehicles. Ocean Engineering, 34, 1607-1617.
- Townsend, N., Sheno, A., 2012. A Gyroscopic Wave Energy Recovery System for Marine Vessels. IEEE Journal of Oceanic Engineering, 37(2), 271-280.
- Townsend, N., Sheno, R., 2014. Control Strategies for Marine Gyrostabilizers, IEEE Journal of Oceanic Engineering, 39(2), 243-255.
- Tomera, M., 2017. Fuzzy self-tuning PID controller for a ship autopilot. Proceedings of the 12th International Conference on Marine Navigation and Safety of Sea Transportation, 93-103, Gdynia, Poland.
- Wahid, N., Hassan, N., 2012. Self-Tuning Fuzzy PID Controller Design for Aircraft Pitch Control. 2012 Third International Conference on Intelligent Systems Modelling and Simulation, Kota Kinabalu, Malaysia.
- Wu, X., Liu, Q., Zhang, K., Xin, X., 2018. Optimal-tuning of proportional-integral-derivative-like controller for constrained nonlinear systems and application to ship steering control. Journal of the Franklin Institute, 355(13): 5667-5689.
- Zhang, X., Yang, J., Zhao, W., Xiao, L., 2016. Effects of wave excitation force prediction deviations on the discrete control performance of an oscillating wave energy converter. Ships Offshore Structure, 11(4), 351-368.
- Zhang, M., Hao, H., Wu, D., Chen, M., Yuan, Z., 2022. Time-optimal obstacle avoidance of autonomous ship based on nonlinear model predictive control, Ocean Engineering, 266, 112591.